Characteristics of an aged organic "brown" aerosol in the urban Po Valley atmosphere

F. Costabile[1], S. Gilardoni[2], F. Barnaba[1], A. Di Ianni[1], L. Di Liberto[1], D. Dionisi[1], M. Manigrasso[3], M. Paglione[2], V. Poluzzi[4], M. Rinaldi[2], M.C. Facchini[2], and G. P. Gobbi[1]

[1]Institute for Atmospheric Sciences and Climate (ISAC), National Research Council (CNR), Rome, Italy
[2]Institute for Atmospheric Sciences and Climate (ISAC), National Research Council (CNR), Bologna, Italy
[3]INAIL, Rome, Italy
[4]ARPA ER, Bologna, Italy

Correspondence to: F. Costabile (f.costabile@isac.cnr.it)

Abstract. We characterize the atmospheric nondust aerosol having the strongest spectral dependence of light absorption (as indicated by the Absorption Angstrom Exponent, AAE) at visible wavelengths in the urban Po Valley. In situ ground measurements of aerosol spectral optical properties, PM_1 chemical composition (HR-ToF-AMS), and coarse and fine size distributions, were carried out in Bologna, and data statistically analysed. Findings prove that a "brown" aerosol (AAE from 2.5 to 6) in the ambient atmosphere is composed by "droplet" mode particles enriched in aged organic aerosol (OA) and nitrate. We provide a comprehensive physico-chemical characterisation of this brown aerosol, including its spectral optical signature, and possible sources. To our knowledge, no previous work has considered these issues in the ambient atmosphere. We compared to literature to put findings in a broader perspective. There is consistency with recent "diluted" urban observations (airborne, and AERONET), and combustion chamber observations. Our study adds to these previous ones that the high AAE values featuring the "brown" aerosol depend on the OA to Black Carbon (BC) ratio more than on OA, and that the link between AAE and OA-to-BC (already observed for freshly emitted primary aerosols from biomass burning) does exist in the ambient atmosphere for this aged "brown" aerosol, as well. The comparison with studies on the composition evolution of OA in the atmosphere strengthens the result that this "brown" aerosol is an aged OA, and provides experimental evidence for the aged "brown" OA formation in the ambient atmosphere. Findings will have important atmospheric implications for modeling studies, and remote sensing observations, as regards the parametrization and identification of Brown OA, and Brown Carbon in the atmosphere.

1 Introduction

Aerosol has an important role in the Earth's climate with both direct and indirect effects; beside that, it affects air quality and atmospheric chemistry. At present, our understanding of the light-absorbing aerosol types is very incomplete (see reviews by Laskin et al., 2015; Moise et al., 2015). An important absorber of solar radiation in the visible region is the atmospheric carbonaceous aerosol (IPCC 2013). Visible-light absorbing properties of this aerosol type vary between two extremes. On one side, there is Black Carbon (BC) that strongly absorbs light over a broad spectral range. On the other side, there is the colourless Organic Carbon (OC) with no absorption or little absorption in the UV spectral range. Between these extremes, there

is a broad range of coloured (moderately volatile) organic compounds that have recently emerged in the scientific literature for their possible role in the Earth's climate. The term "brown carbon" (BrC) has emerged to describe this aerosol having an absorption spectrum smoothly increasing from the vis to the near-UV wavelengths, with a strong wavelength dependance of the light absorption coefficient ($\lambda^{-2} - \lambda^{-6}$) (Andreae and Gelencsér, 2006; Moosmüller et al., 2011; Bond et al., 2013; Laskin et al., 2015; Moise et al., 2015). In fact, BrC lacks a formal analytical definition (Bond et al., 2013). In this study, we will refer to a "brown" aerosol to indicate an aerosol type with high values (2-6) of the Absorption Ångström Exponent (AAE), a parameter describing the wavelength (λ) dependent absorption coefficient (σ_a) of light by aerosol, written as:

$AAE(\lambda) = -\frac{dln(\sigma_a)}{dln(\lambda)}$.

What is known about the BrC aerosol is that it is an organic matter having both primary and secondary sources (Laskin et al., 2015). Primary BrC can be emitted together with BC from low-temperature combustion processes, like wood combustion (Andreae and Gelencsér, 2006). Secondary organic aerosol (SOA) formed in the atmosphere contributes to the light absorbing carbon, as well (Moise et al., 2015). Little is known about sources of the secondary BrC associated to SOA (Saleh et al., 2013; Zhang et al., 2013).

Numerous evidences indicate increased absorption towards UV for aerosol particles having high nitrate (e.g., Zhang et al., 2013; Jacobson, 1999) and sulfate contents (Powelson et al., 2014; Lin et al., 2014; Lee et al., 2013; Song et al., 2013). Lin et al. (2014) reported the formation of light-absorbing SOA constituents from reactive uptake of isoprene epoxydiols onto preexisting acidified sulfate seed aerosol as a potential source of secondary BrC under tropospheric conditions. Powelson et al. (2014) discussed the BrC formation by aqueous-phase carbonyl compound reactions with amines and ammonium sulfate. Lee et al. (2013) studied the likely and unkown effect of sulfate on the formation of light absorbing materials and organo-nitrogen via aqueous glyoxal chemistry in aerosol particles. Song et al. (2013) observed significant light absorption at 355 and 405 nm for the SOA formed from an α-pinene + O_3 + NO_3 system only in the presence of highly acidic sulfate seed aerosols under dry conditions. Several studies demonstrated the importance of ammonium, both as a catalyst and as a reactant, in the formation of light-absorbing products (Laskin et al., 2015; Powelson et al., 2014). SOA formation can occur both in the gas and condensed phase. Recently, an efficient SOA production has been recognised in cloud/fog drops and water containing aerosol: water soluble products of gas phase photochemical reactions may dissolve into an aerosol aqueous phase and form SOA through further oxidation, this SOA being referred to "aqSOA" (Ervens et al., 2011; Laskin et al., 2015). AqSOA formation impacts total SOA mass, and aerosol size distributions by adding mass to the so-called "droplet mode" (Ervens et al., 2011). Meng and Seinfield (1994) showed that the aerosol "droplet mode" in urban areas is the result of activation of smaller particles to form fog, followed by aqueous-phase chemistry, and fog evaporation. It was demonstrated that aqSOA formation can affect aerosol optical properties by adding light-absorbing organic material at UV wavelengths (Shapiro et al., 2009; Ervens et al., 2011).

Despite the efforts made, relations between optical properties and chemical composition of organic compounds with spectrally variable light absorption (high AAE) are poorly understood (Laskin et al., 2015). A number of previous works (Shinozuka et al, 2009; Russell et al., 2010; Arola et al., 2011) studied how the organic aerosol (OA) mass fraction (f_{OA}) relates to AAE, and to Single Scattering Albedo (SSA), the ratio of scattering to extinction, a key parameter to understand aerosol warming or cooling effect. Results from in situ measurements on the C-130 aircraft mostly over Central Mexico during MILAGRO (Russell

et al., 2010) showed that both Organics and dust increase AAE values. Russell et al. (2010) showed a direct correlation between AAE and f_{OA}, the larger particles (dust) having higher AAE, and the smaller particles (pollution related) having lower AAE. On the basis of the same data, Shinozuka et al (2009) showed that AAE generally increases as f_{OA} or SSA increases. This was explained by the presence of humic like substances (HULIS) and dust, which are colored (high AAE), weak absorbers (high

5   SSA), with high f_{OA}. Very recently, Saleh et al. (2014) burnt a selection of biomasses in a combustion chamber, varying the combustion parameters to obtain a range of BC-to-OA ratios. This ratio, the relative proportions of BC and OA mass, depends on fire characteristics, and determine its colour from black to brown to white as the ratio decreases (Bellouin , 2014). Their findings link the extent of absorbance to the BC-to-OA ratio for aged and fresh biomass burning aerosols. If confirmed by further studies, this link can be a potentially strong predictive tool for light-absorbing properties of biomass burning aerosols

10   (Bellouin , 2014; Moise et al., 2015). Following the Saleh et al. (2014)'s idea, Lu et al. (2015) reviewed available emission measurements of biomass burning and biofuel combustion, and found similar results indicating that AAE of the bulk OA decreases with the BC-to-OA ratio. They conclude that the absorptive properties of OA from biomass/ biofuel burning depend strongly on burning conditions and weakly on fuel types and atmospheric processing.

In this study, we characterize the nondust aerosol having the strongest spectral dependance of light absorption (as indicated

15   by the AAE) at visible wavelengths in the ambient atmosphere. In situ ground ambient measurements of chemical (HR-ToF-AMS), optical (3-λ nephelometer and PSAP), and micro-physical (SMPS and APS) aerosol properties were taken in Bologna, Po Valley, together with ancillary observations (including ceilometer retrievals). Major features of the "brown" aerosol in the ambient urban atmosphere are investigated. We used a global approach where the aerosol type, as a whole, is linked to the highest AAE values. We investigate sources of this brown aerosol by relating AAE to primary and secondary aerosol

20   populations extracted through a statistical analysis of size distribution, and mass spectral features. We then characterise physico-chemical properties of the observed brown aerosol, and illustrate a case-study. Findings are then discussed in comparison with previous literature works to explore their general validity instead of treating them like results of a local study.

2   Experimental

Optical, chemical, and microphysical aerosol properties were measured, in the framework of the ARPA ER Supersite project, at

25   the urban background site of Bologna (44 ° 31' 29" lat, 11° 20' 27' lon), in the Po Valley (Italy). Two measurement campaigns lasting one month were taken: October 22 - November 13, 2012 (Fall campaign), and February 1-27, 2013 (Winter campaign). Measurements performed are detailed below.

2.1   Measurement cabins and sampling lines

Equipment was set up in two different cabins, located side by side. Optical properties and coarse fraction size distributions

30   were measured in the same cabin, all the instruments set-up on the same inlet system equipped with a PM_{10} head. External air was pumped in the cabin into a stainless steel tube (length = 4.0 m) by an external pump ensuring a laminar flow (Reynolds number <2000). The cabin was conditioned at 20-25°C. The difference between air temperature and dew point was enough to

dry sampled air. Chemical properties and fine and ultrafine particle number size distribution were measured through a separate stainless steel inlet tube equipped with a PM$_1$ head.

2.2 Optical Measurements

Spectral optical properties in the visible range were measured online with a 5 minute time resolution. The dry aerosol absorption coefficient, $\sigma_a(\lambda)$, at three wavelengths ($\lambda =$, 467, 530, 660 nm) was measured by a 3-wavelength particle soot absorption photometer (PSAP, Radiance Research). Raw PSAP data were corrected according to previous work by Bond et al. (1999); Virkkula et al. (2005); Virkkula (2010). The correction procedure requires wavelength resolved scattering coefficients ($\sigma_s(\lambda)$), which were derived from measurements of the dry aerosol $\sigma_s(\lambda)$ at 450, 525, and 635 nm, performed by an integrating nephelometer (Ecotech, mod. Aurora 3000). All measurements with $\sigma_a(\lambda) < 1$ Mm^{-1}, and $\sigma_s(\lambda) < 10$ Mm^{-1} were eliminated to reduce possible experimental errors from the dataset.

2.3 Chemical Measurements

Chemical composition of atmospheric aerosol particles were characterized online with a High Resolution Time of Flight Aerosol Mass Spectrometer (HR-ToF-AMS, Aerodyne Research Inc., Billerica) (DeCarlo et al., 2006). The HR-ToF-AMS measured the chemical composition of non-refractory PM$_1$ (nr-PM$_1$), i.e sulfate, nitrate, ammonium, chloride, and organic aerosol. The instrument alternated acquisition in V-mode (higher sensitivity and lower mass spectral resolution), and W mode (lower sensitivity and higher mass spectral resolution) every 2.5 minutes. Quantitative information discussed here corresponds to the data collected in V mode. While operating in the V mode, the instrument measures particle size distribution based on their time of flight (Jimenez et al., 2003). HR-ToF-AMS data were analyzed using SQUIRRELL v1.51 and PIKA v1.10 software (D. Sueper, University of Colorado, Boulder, Boulder, CO, USA) within Igor Pro 6.2.1 (WaveMetrics, Lake Oswego, OR). Collection efficiency was calculated according to Middlebrook et al. (2012) based on aerosol chemical composition, and relative humidity. Data validation was performed by comparison with offline measurements of sulfate, ammonium, and nitrate concentrations in PM$_1$ aerosol samples. The HR-ToF-AMS aerosol sample line was dried below 40% RH with a Nafion drier.

2.4 Particle Number Size distributions

Particle number size distributions (PNSDs) were measured by combining a commercial Scanning Mobility Particle Sizer (SMPS, TSI mod. 3080 with Long-DMA, TSI mod. 3081, equipped with a water-based Condensation Particle Counter, CPC, TSI mod. 3787), and a commercial Aerodynamic Particle Sizer (APS, TSI). Particles from 14 nm to 750 nm of mobility diameter were sized and counted by the SMPS; particles from 0.5 to 20 μm of aerodynamic diameter were sized and counted by the APS (the procedure to fit the two PNSDs is described in the Sect.3.2). SMPS data were corrected for penetration errors through the sampling line, penetration efficiency due to diffusion losses (calculated according to Hinds (1999)) being higher than 98% for particles bigger than 14 nm. An impactor (nozzle of 0.457 μm) was used to remove larger particles.

3 Data analysis

Data measured by all the instruments were merged in a single dataset of 5 minute resolution. The dataset consisted of 11211 records (5764 in fall, and 5447 in winter), including 2551 records (covering 40 days of measurements) with no missing value, and 1087 records (150 in fall, and 937 in winter) of cleaned data after data analysis.

3.1 Inference of the optical Black Carbon mass concentration

A wavelength (λ) dependent BC absorption coefficient ($\sigma_{aBC}(\lambda)$), and equivalent BC mass concentration, were calculated. The measured absorption coefficient at 660 nm ($\sigma_a(660)$) was used to derive $\sigma_{aBC}(530)$, and then the BC mass concentration, assuming: (i) $AAE_{530-660}$ of σ_{aBC} to be 1, and (ii) BC Mass Absorption Efficiency at 530 nm to be 10 m^2 g^{-1} (see Costabile et al. (2015) for more details). We discarded data possibly affected by desert dust (43 records over 5 days of measurements) to ensure that the equivalent BC mass concentration is not affected from contamination by desert dust. Dust presence was identified based on the information provided by the bulk aerosol spectral optical properties (Russell et al., 2010). In particular, we fixed threshold on the Scattering Angstrom Exponent (SAE), the AAE, and the Single Scattering Albedo (SSA) (Costabile et al., 2013).

3.2 Fitting procedure for the particle number size distribution

Data of particle number size distributions (PNSDs) were measured by two different instruments (SMPS and APS, Sect.2). These data were merged to obtain one PNSD based on particle electrical mobility diameters (d_m) ranging from 14 nm to 14 μm. PNSDs measured by APS are based on aerodynamic diameters (d_a); these data were converted to PNSDs based on d_m according to Eq.1 (Khlystov et al., 2004; Seinfeld and Pandis, 2006):

$$d_m = \chi \frac{C_c(d_m)}{C_c(d_a)} \frac{d_a}{(\frac{\rho_p}{\rho_0 \chi})^{1/2}} \tag{1}$$

where χ is the shape factor, $C_c(d_m)$ and $C_c(d_a)$ are the slip correction factors based on d_m and d_a respectively, ρ_p is the particle density, and ρ_0 is the unit density (1 $g \cdot cm^{-3}$). In applying Eq.1 to convert APS data, we assumed: particle diameter (d_p) = d_m; $C_c(d_m)$ = 1 and $C_c(d_a)$ = 1 (continuum regime); χ = 1 (spherical particles); ρ_p continuously varying from 1.6 to 2 $g \cdot cm^{-3}$.

PNSDs measured by SMPS and APS overlap for d_m ranging from 460 to 593 nm. The two PNSDs were then fitted by a power-law function (Junge size distribution) (Khlystov et al., 2004; Seinfeld and Pandis, 2006), meaning that the lognormal PNSD defined in Eq.2:

$$n_N(log_{10}d_m) = \frac{dN}{dlog_{10}(d_m)}, \tag{2}$$

is assumed to vary according to Eq.3:

$$n_N(log_{10}d_m) = \frac{c}{d_m^{\alpha}}, \tag{3}$$

where c and α are two coefficients. The following iterative procedure was used to correct data when APS lognormal PNSD differed by more than 0.1 cm^{-3} from SMPS lognormal PNSD: (i) the coefficient c is randomly initialized from 0 to 1000; (ii) the value of α is calculated by Eq.3 assuming a value from 2 to 5 typical of atmospheric aerosol (Seinfeld and Pandis, 2006); (iii) the fitted lognormal PNSD is calculated by Eq.3; (iv) results are constrained by minimizing mean square error between

5 calculated lognormal PNSD and APS lognormal PNSD, and maximising correlations between SMPS lognormal PNSD and APS lognormal PNSD. Fitted PNSDs were further corrected by visual inspection through a smoothing procedure, and suspected cases eliminated. The final dataset contained PNSD data based on d$_m$ from 14.1 to 429.4 nm measured by the SMPS, from 446.1 to 699 nm generated by the fitting procedure, and from 0.7 to 14 μm measured by the APS .

4   Results and discussion

10 In this section, we first identify a "brown" aerosol (AAE from 2 to 6) by relating AAE to key aerosol populations extracted through a combined statistical analysis of PNSD, and organic aerosol mass spectra. We then characterise physico-chemical properties of the observed "brown" aerosol as regards number and mass size distribution (and relevant modes), and major PM$_1$ chemical components (BC, organics, nitrate, ammonium, and sulfate), relevant mass fractions, and ratios. A case-study is finally illustrated.

15 ### 4.1   A "brown" aerosol type: identification and features

Key aerosol types were identified through a statistical approach. PNSD principal components (PCs) were identified by Principal Component Analysis (PCA). PCA was calculated following the findings of a previous long-term study over multiple sites (8 concurrent stations) by Costabile et al. (2009). Four principal components (PC1-PC4) were extracted, explaining 90% of the variance. We interpreted these PCs based on: (i) their statistical properties, i.e. "scores" and "loadings" (loadings indicate

20 correlations between PNSDs and PCs, i.e. the "mode" of the PNSD associated to the PC); (ii) Pearson's correlation coefficients (r) shown in Table 1, between PCs, AAE, and PM$_1$ mass fractions of BC, organics, nitrate, sulfate, and ammonium (f$_{BC}$, f$_{OA}$, f$_{NO3}$, f$_{SO4}$, f$_{NH4}$). The median diameter of the particle surface size distribution (d$_{med(S)}$) in Table 1 is intended to add information on optically relevant aerosol sizes. The coupling of BC mass concentration and f$_{BC}$ in Table 1 is intended to give information on BC particle size. BC mass concentration was assumed to increase mostly with increasing concentration

25 of larger BC particles, as mass depends on volume (BC mass concentration of accumulation mode BC particles is larger than that of soot mode BC particles, all other things being equal). Higher f$_{BC}$ values were assumed to characterize freshly emitted BC particles, as atmospheric ageing increases non-BC particle coating (thus decreasing f$_{BC}$). Higher f$_{BC}$ values coupled to lower BC mass concentration were, therefore, interpreted as indicators of ultrafine BC particles, and vice versa. The OA to BC ratio (OA-to-BC) in Table 1 is intended to indicate both combustion characteristics (higher for biofuels than for fossil fuel

30 combustion), and aerosol ageing (lower for fresh aerosols) (Saleh et al., 2014; Bond et al., 2013). Correlations to f$_{43}$ and f$_{44}$ (defined as the ratio of the AMS signal at m/z 43 and m/z 44, respectively, to the total organics AMS signal) in Table 1 are

intended to add information on the oxidised OA. The higher the f_{44}, the more oxidised the OA; the higher the f_{44}/f_{43} ratio, the lower the volatility of this oxidised OA (Ng et al., 2010, 2011; Moise et al., 2015).

PC1, PC2, and PC4 represent primary aerosol sources. PC1 is a fine-mode BC aerosol: it correlates to BC, inversely to f_{44} (the lower f_{44}, the more the aerosol approaches the hydrocarbon-like OA), the PNSD mode peaking from 100 to 200 nm. PC2 and PC4 are ultrafine primary aerosols (both correlate to f_{BC}, their PNSD modes peaking from 20 to 100 nm, and from 10 to 40 nm, respectively). The remaining PC3 (10% of the variance) relates to a secondary aerosol: it is the only PC inversely correlated to f_{BC}, and directly correlated to f_{OA}, f_{44}, OA-to-BC, and $d_{med(S)}$. Figure 1 shows the PNSD "mode" of this PC (brown line). The PNSD mode of PC3 is exactly the same as that identified by Costabile et al. (2009) for the aerosol "droplet mode" (green, blue, red, and black lines in Fig. 1). The aerosol "droplet mode" is one of the two aerosol accumulation modes (the smaller one is the condensation mode, the larger one is the droplet mode), shown to form from activation of condensation mode particles, formation of cloud/fog drops, followed by aqueous-phase chemistry, and droplet evaporation (John, 1990; Meng and Seinfield , 1994; Seinfeld and Pandis, 2006).

In Table 1, it is indicated a robust statistical relation linking AAE, this "droplet" mode component (PC3), and OA-to-BC, together with f_{OA}, $d_{med(S)}$, f_{44} and f_{43}. Figure 2 shows this relation. When the droplet mode PC scores positive (PC scores >0 indicate that this aerosol type forms), the AAE is greater than 2.5. Both AAE and droplet mode increase with increasing OA-to-BC, and f_{44}, both indicators of OA aged in the atmosphere (Ng et al., 2010; Bond et al., 2013). Data, therefore, identify a "brown" aerosol type, i.e. an aerosol showing AAE from 2.5 to 6, having high "droplet" mode PC scores. The dependence of this "brown" aerosol on PM_1 major costituents, and relevant ratios, is illustrated in Fig. 3 and Fig. 4, where the brown aerosol formation is indicated by the combined increase of AAE (y-axis) and droplet mode PC score (marker color). This "brown" aerosol formation depends on the organic mass fraction (f_{OA}, Fig.3a), and is inversely correlated to the mass fractions of BC (f_{BC}, Fig.3b), and sulfate (f_{SO4}, Fig.3c). The dependence on the nitrate mass fraction (f_{NO_3}, Fig.3d) is not obvious, as high AAE values and droplet mode scores are observed for both $f_{NO_3} <0.05$ and $f_{NO_3} \simeq 0.25$. The relation between this "brown" aerosol and the BC-to-OA ratio (or its inverse OA-to-BC ratio = f_{OA}/f_{BC}) is shown in Fig. 4. The area showing the brown aerosol (AAE from 2.5 to 6.6, positive droplet mode PC scores) has high OA-to-BC ratios (note correlation r = 0.78 between AAE and OA-to-BC ratio, Table 1). The inverse dependence between this "brown" aerosol formation and the BC-to-OA ratio confirms results of the statistical analysis (correlations with f_{44} and f_{43}) indicating that the brown aerosol is an aged OA. Indeed, it is typical that BC contribution declines, and OA contribution increases, as the smoke aerosol ages in the atmosphere.

Taken together, findings finally suggest that the "brown" aerosol type observed in the Po Valley is mainly composed of aged OA in "droplet" mode particles.

4.2 A case study for the "brown" aerosol

We present here a case study to visualize main aerosol features of the "brown" aerosol observed. The values of this case study were indicated in Fig. 4 by "*": they represent the highest values of AAE, and droplet mode PC scores observed, and thus a case of brown aerosol formation. Figure 5 (panels a, b, c) compares mean values of volume and mass size distributions measured over the whole field experiment with relevant values measured during this case study (first of February, 2013 from 17:30 to

19:00). Relative humidity (RH) was high (97.5±0.4%, against a mean value for the winter campaign of 82 ± 14 %, and a maximum of 98 %), temperature averaged 2.8 ± 0.0 ° C (campaign mean value=3.5 ± 2.8 ° C). Aerosol vertical profiles from a LD40 ceilometer (Fig. 5d) indicate a foggy day, except for the middle part of the day (from 11:00 to 15:00) when the fog layer is shown to dissipate. The day started with low concentrations of sub-micrometer aerosol particles (Fig. 5e). Coarse mode

5 aerosol particles increased in the early hours of the day, and then decreased, followed by the increase of droplet mode aerosol particles (as indicated by the area in Fig. 5e corresponding to diameters ranging from 500 to 800 nm, and PC3 scores - not shown here). We interpret this as formation of fog drops, followed by droplet evaporation, and aerosol droplet mode formation, a plausible mechanism for formation of this aerosol type (John, 1990; Meng and Seinfield , 1994; Seinfeld and Pandis, 2006). AAE (Fig. 5f) was significantly higher than its mean value (up to more than 6 - unfortunately no data is available before 15:00).

10 Relevant volume size distribution (Fig. 5a) is centered on the droplet mode (d_m from 450 to 700 nm), the peak being more than four times as high as that of the mean value. Mass size distributions of the main constituents of nr-PM$_1$ (NO$_3$, organics, and NH$_4$) are centered around 700 nm of the vacuum aerodynamic diameter (d_{va}). Note that d_{va} = 700 nm corresponds to d_m = 468 nm for spherical particles with $\rho_p = 1.5 g \cdot cm^{-3}$ in the continuum regime, as d_m and d_{va} are linked by Eq.4 (Seinfeld and Pandis, 2006) :

$$d_{va} = d_m \frac{\rho_p}{\rho_0}. \tag{4}$$

In addition, the organic aerosol mass below d_{va} = 300 nm was significantly lower than that of the droplet mode, especially when compared to the average field results (Fig. 5c). Relevant absorption and scattering coefficients (not shown here) ranged from 5 to 10 Mm^{-1}, and from 300 to 400 Mm^{-1}, respectively. As shown by this case study, a general feature of the whole field campaign was that the brown aerosol formed in the early afternoon.

20 ## 5   Discussion in comparison with previous works

In this section, we discuss findings to explore consistency with literature, and put results in a broader perspective.

5.1   The "brown" aerosol in the ambient atmosphere

In Figure 6, relations illustrated in Fig.3 and Fig. 4 between AAE, f$_{OA}$, and f$_{OA}$/f$_{BC}$ = OA-to-BC, are compared to literature. Our results (obtained in urban ambient air) are compared to previous findings obtained under "diluted" urban conditions (air-

25 borne, and AERONET columnar observations) (Shinozuka et al, 2009; Russell et al., 2010; Arola et al., 2011), or in combustion chambers experiments (Saleh et al., 2014; Lu et al., 2015).

Figure 6a shows the relation between AAE (y axis), f$_{OA}$ (x axis), SSA (at 530 nm, marker color), and $d_{med(S)}$ (marker size). The Pearson's correlation coefficient (r) is 0.56. Fig. 6a is intended to compare to Russell et al. (2010)'s results, indicated by the black line. These results showed that increasing f$_{OA}$ values are accompanied by increasing AAE values when dust is absent.

30 The pattern of our data is similar, although most of our data points (that are ground in situ measurements) lie above Russell et al. (2010)'s line (that were airborne measurements). As in the case of Russell et al. (2010)'s work, our data make evident

that there are conditions when AAE increases irrespective of f_{OA}. In contrast, when f_{OA} is normalised to f_{BC} (f_{OA}/f_{BC} = OA-to-BC ratio), there is a strong correlation with AAE (r = 0.78, Fig. 6b). The increasing OA-to-BC ratio is accompanied by a uniform increase of AAE. As well, there is a weak increase of SSA (r = 0.56), and $d_{med(S)}$ (r = 0.49). Note values measured during the case study (Fig. 5) indicated by "*". This comparison suggests that: (i) the "brown" aerosol formation might be

5 observed by airborne and AERONET observations, as well as by ground measurements, and (ii) the OA-to-BC ratio indicates this formation, and related AAE increase, better than f_{OA} does.

Saleh et al. (2014) used the inverse of OA-to-BC to parametrize the AAE of biomass burning emissions in a combustion chamber experiment. To compare to Saleh et al. (2014)'s work, panel c of Fig. 6 shows AAE versus BC-to-OA (the inverse in log scale of the x axis in Fig. 6b). The line in Fig. 6c indicates Saleh et al. (2014)'s least-square-fit. A similar pattern is

10 evident, although the highest AAE values observed in our study (up to 6.6) were not obtained in the chamber experiment (up to 3.5). Similar results were confirmed by Lu et al. (2015). Both Saleh et al. (2014) and Lu et al. (2015) concluded that this dependence of AAE on the BC-to-OA ratio can be observed solely for biomass burning OA, and not for fossil fuel OA. Note that when AAE >3.5, SSA is higher than 0.98 (Fig. 6), all values of the case study being associated with these high AAE. This comparison strenghtens our findings indicating that the "brown" aerosol (i) represents an aerosol aged in the atmosphere,

15 and (ii) is not a freshly emitted aerosol, as it is not observed in a combustion chamber experiment. If Saleh et al. (2014)'s results are confirmed, this comparison suggests that this brown aerosol derives from the processing of biomass burning OA. It is worth noting that the AAE of this secondary brown aerosol would be two times higher than that of the fresh biomass burning OA it likely derives from. Lu et al. (2015)'s experiments similarly suggested that atmospheric processing should not decrease biomass burning OA absorptive properties.

20 **5.2 Spectral optical properties of the "brown" aerosol**

In this section, we discuss if the "brown" aerosol can be the unambiguously identified by its spectral optical properties. In a previous work, Costabile et al. (2013) obtained a paradigm to classify urban aerosol types, based on a proper combination of their AAE, SSA, and SAE in the visible region: SAE was plotted against AAE times dSSA (= SSA spectral variation). In panel (a) of Fig. 7, we show this paradigm for the "brown" aerosol (represented by the experimental data of the droplet mode) in

25 comparison to key urban aerosol types (represented by Mie simulated data). Panel (b) is intended to show the variability of relevant spectral optical properties with varying mass fractions of PM_1 major components.

Figure 7a shows that there is an unequivocal spectral signature in the visible region for the "brown" aerosol: (i) AAE from 2.5 to 6, (ii) SSA from 0.9 to 1, always increasing with increasing wavelength (λ), (iii) SAE from 0.5 to 2. This signature is in line with that of the "large organic mode" (LOM). LOM was obtained by simulating: (i) a monomodal PNSD, the mode

30 peaking in the 300-800 nm size range (like the droplet mode PNSD in Fig. 5a); (ii) spectral refractive indices (k_λ) of k_{467} = 1.460-0.012i, k_{530} = 1.454-0.008i, and k_{660} = 1.512-0.0075i. This comparison suggests to extrapolate k_λ values of LOM for the "brown" aerosol. It is reasonable that real k_λ values vary much more than simulated ones: numerical simulations represent pure aerosols (pure aerosols have constant k_λ), while experimental data represent mixed aerosols (mixed aerosols have variable k_λ). However, the resulting average $k_{530} = 8 \cdot 10^{-3}$ for the "brown aerosol", associated to AAE values from 3 to 6, is fully consistent

with literature k values recently reviewed by Lu et al. (2015). This result means that visible light absorption properties by the "brown aerosol" have to be carefully considered, and should not be ignored.

5.3 A SOA type "brown" aerosol

Findings indicate a relation linking the "brown" aerosol to the aged OA. AMS measurements enable to map OA ageing level by combining f_{43} and f_{44} (Sect. 4.1, and Table 1), representing intensities of the two oxygen-containing ions domining the OA spectra (see review by Moise et al., 2015). f_{44} has been found to originate from the dissociation in the AMS of oxidised organic molecules (the CO_2^+ fragment from carboxylic acid groups). f_{43} has been related to non-acid oxidised species (the $C_2H_3O^+$ fragment from aldehydes and ketones), in addition to saturated hydrocarbons (the $C_3H_7^+$ fragment). Figure 8 shows f_{44} plotted against f_{43}, and their relation with the brown aerosol (AAE is data color, the droplet mode PC score is data size). This figure is intended to reproduce the "triangle plot" proposed by Ng et al. (2011, 2010), which encompasses the majority of OA values measured in ambient samples. It is showed that the "brown" aerosol (the largest yellow-to-red markers) lies in the oxidised OA region, where most of the semi volatile oxidised OA measurements taken at the ground lie (Ng et al., 2010; Crippa et al., 2014). The composition found for this "brown" aerosol (high organics, nitrates and ammonium, Fig.5) is coherent with numerous previous studies showing an increased light absorption towards UV for SOA particles (Jacobson, 1999; Lee et al., 2013; Song et al., 2013; Zhang et al., 2013; Powelson et al., 2014; Lin et al., 2014; Laskin et al., 2015).

This comparison reinforces our hypothesis that the "brown" aerosol is an aged OA.

6 Summary and conclusions

We characterized the nondust aerosol having the strongest spectral dependance of light absorption (as indicated by the Absorption Angstrom Exponent, AAE) at visible wavelengths in an urban ambient atmosphere of the Po Valley (Bologna). In situ ground ambient measurements of chemical (HR-ToF-AMS), optical (3-λ nephelometer and PSAP), and micro-physical (SMPS and APS) aerosol properties were taken, together with ancillary observations (including ceilometer retrievals).

Findings prove that a "brown" aerosol (AAE from 2.5 to 6) forms in the ambient atmosphere, and that this "brown" aerosol is composed by "droplet" mode particles enriched in aged organic aerosol (OA) and nitrate. We provide a comprehensive physico-chemical characterisation of this brown aerosol, including its spectral optical properties.

We first identified a specific aerosol type having high AAE values (2.5-6.6), and called it "brown" aerosol. We investigated its major sources in the urban atmosphere by relating AAE to key aerosol populations extracted through a statistical analysis of aerosol size distribution. We then characterised physico-chemical properties of this "brown" aerosol as regards number and mass size distribution (and relevant modes), major PM_1 chemical components (BC, organics, nitrate, ammonium, and sulfate), their mass fractions, and relevant ratios (including the BC-to-OA ratio). A case-study was illustrated. It turned out that the "brown" aerosol: (i) is a "droplet" mode aerosol (its monomodal number size distribution peaking at 450-700 nm), (ii) is aged OA, and (iii) can be identified by higher values of the OA-to-BC ratio. To our knowledge, no previous work has considered

these issues in the ambient atmosphere. This is the first experimental evidence that extends observations by Saleh et al. (2014) to ambient conditions, and provides a micro-physical characterization of this "brown" aerosol.

Consistency of findings with literature was then explored. We compared our results with previous findings obtained for "diluted" urban aerosols (airborne and AERONET observations), and freshly emitted aerosols (combustion chamber experiments).

5 We found a dependence of AAE on OA similar to what found for airborne and AERONET data, and a dependence of AAE on the BC-to-OA ratio similar to what found for freshly emitted aerosols. Our study adds to these previous studies that: (i) AAE depends on the OA-to-BC ratio more than on OA, and (ii) the link between AAE and the OA-to-BC (already observed for the freshly emitted primary aerosol from biomass burning) is observed in the ambient atmosphere, as well, where it can be used to identify the "brown" aerosol. Finally, the comparison with a simulation work allowed to obtain the following optical signature

10 in the visible region for the "brown" aerosol: AAE of 2.5-6.6, SAE of 0.5-2, SSA of 0.9-1, and average refractive index at 467 nm of 1.460-0.012i.

Findings will have important atmospheric implications for modeling studies, and remote sensing observations. The link between AAE and the OA-to-BC ratio can be a strong tool to parametrize the "brown" aerosol in the atmosphere, as well as to investigate brown OA and Brown Carbon. It is worth noting that this link can be used to extrapolate preliminary chemical

15 information from optical ones, as optical techniques are increasingly used to characterise aerosol properties.

Acknowledgements. This work was realized in the framework of the Supersito Project. The work was partly accomplished in the framework of the DIAPASON ("Desert-dust Impact on Air quality through model-Predictions and Advanced Sensors ObservatioNs") project, funded by the European Commission (LIFE+ 2010 ENV/IT/391).

References

Andreae, M. O. and Gelencsér, A.: Black carbon or brown carbon? The nature of light-absorbing carbonaceous aerosols, Atmos. Chem. Phys., 6, 3131-3148, doi:10.5194/acp-6-3131-2006, 2006.

Arola, A., Schuster, G., Myhre, G., Kazadzis, S., Dey, S., and Tripathi, S. N.: Inferring absorbing organic carbon content from AERONET data, Atmos. Chem. Phys., 11(1), 215-225, 2011.

Bellouin, N.. Aerosols: The colour of smoke, Nat. Geosci., 7(9), 619-620, 2014.

Bond, T. C., Anderson, T. L., and Campbell, D.: Calibration and intercomparison of filter-based measurements of visible light absorption by aerosols, Aerosol Sci. Tech., 30, 582-600, 1999.

Bond, T.C., Doherty, S.J., Fahey, D.W., Forster, P. M., Berntsen,T., DeAngelo, B.J., Flanner, M.G., Ghan,S., Kärcher, B., Koch, D., Kinne, S., Kondo, Y., Quinn, P.K., Sarofim, M.C., Schultz, M.G., Schulz, M., Venkataraman, C., Zhang, H., Zhang, S., Bellouin, N., Guttikunda, S. K., Hopke, P. K., Jacobson, M. Z., Kaiser, J. W., Klimont, Z., Lohmann, U., Schwarz, J. P., Shindell, D., Storelvmo, T., Warren, S.G., Zender, C.S.: Bounding the role of black carbon in the climate system: A scientific assessment, J. Geophys. Res. Atmos., 118, 5380-5552, doi:10.1002/jgrd.50171, 2013.

Costabile, F., Birmili, W., Klose, S., Tuch, T., Wehner, B., Wiedensohler, A., Franck, U., König, K., and Sonntag, A.: Spatio-temporal variability and principal components of the particle number size distribution in an urban atmosphere, Atmos. Chem. Phys., 9, 3163-3195, doi:10.5194/acp-9-3163-2009, 2009.

Costabile, F., Barnaba, F., Angelini, F., and Gobbi, G. P.: Identification of key aerosol populations through their size and composition resolved spectral scattering and absorption, Atmos. Chem. Phys., 13, 2455-2470, doi:10.5194/acp-13-2455-2013, 2013.

Costabile, F., Angelini, F., Barnaba, F., Gobbi, G. P.: Partitioning of Black Carbon between ultrafine and fine particle modes in an urban airport vs. urban background environment, Atmos. Environ., 102, 136-144, 2015.

Crippa, M., Canonaco, F., Lanz, V. A., Äijälä, M., Allan, J. D., Carbone, S., Capes, G., Ceburnis, D., Dall'Osto, M., Day, D. A., DeCarlo, P. F., Ehn, M., Eriksson, A., Freney, E., Hildebrandt Ruiz, L., Hillamo, R., Jimenez, J. L., Junninen, H., Kiendler-Scharr, A., Kortelainen, A.-M., Kulmala, M., Laaksonen, A., Mensah, A. A., Mohr, C., Nemitz, E., O'Dowd, C., Ovadnevaite, J., Pandis, S. N., Petäjä, T., Poulain, L., Saarikoski, S., Sellegri, K., Swietlicki, E., Tiitta, P., Worsnop, D. R., Baltensperger, U., and Prévôt,, A. S. H.: Organic aerosol components derived from 25 AMS data sets across Europe using a consistent ME-2 based source apportionment approach, Atmos. Chem. Phys., 14, 6159-6176, doi:10.5194/acp-14-6159-2014, 2014.

DeCarlo, P. F., Kimmel, J. R., Trimborn, A., Northway, M. J., Jayne, J. T., Aiken, A. C., Gonin, M., Fuhrer, K., Horvath, T., Docherty, K. S., Worsnop, D. R., and Jimenez, J. L.: Field-deployable, high-resolution, time-of-flight aerosol mass spectrometer, Anal. Chem., 78, 8281-8289, 2006.

Ervens, B., Turpin, B. J., and Weber, R. J.: Secondary organic aerosol formation in cloud droplets and aqueous particles (aqSOA): a review of laboratory, field and model studies, Atmos. Chem. Phys., 11, 11069-11102, doi:10.5194/acp-11-11069-2011, 2011.

Hinds W.C., Aerosol Technology, 2nd, Edition., Wiley, New York, 1999.

Khlystov, A., Stanier,C., Pandis, S. N.: An Algorithm for Combining Electrical Mobility and Aerodynamic Size Distributions Data when Measuring Ambient Aerosol, Special Issue of Aerosol Science and Technology on Findings from the Fine Particulate Matter Supersites Program., Aerosol Sci. Tech., 38, S1, 229-238, 2004.

Laskin, A., Laskin, J., and Nizkorodov, S. A.: Chemistry of Atmospheric Brown Carbon, Chem. Rev., doi: 10.1021/cr5006167, 2015.

Lee, A.K.Y., Zhao, R., Li, R., Liggio, J., Li, S.-M., Abbatt, J.P.D.: Formation of light absorbing organo-nitrogen species from evaporation of droplets containing glyoxal and ammonium sulfate, Environ. Sci. Technol., 47 (22), 12819-12826, doi:10.1021/es402687w, 2013.

Lin, Y.-H., Budisulistiorini, S.H., Chu, K., Siejack, R.A., Zhang, H., Riva, M., Zhang, Z., Gold, A., Kautzman, K.E., Surratt, J.D.: Light-absorbing oligomer formation in secondary organic aerosol from reactive uptake of isoprene epoxydiols, Environ. Sci. Technol., 48 (20), 12012-12021, doi: 10.1021/es503142b, 2014.

Lu, Z., Streets, D.G., Winijkul, E., Yan, F., Chen, Y., Bond, T.C., Feng, Y., Dubey, M.K., Liu, S., Pinto, J.P., Carmichael, G.R.: Light absorption properties and radiative effects of primary organic aerosol emissions, Environ. Sci. Technol., 49 (8), 4868-4877, doi: 10.1021/acs.est.5b00211, 2015.

Jacobson, M. Z.: Isolating nitrated and aromatic aerosols and nitrated aromatic gases as sources of ultraviolet light absorption, J. Geophys. Res. - Atmos., 104(D3), 3527-3542, 1999.

Jimenez, J. L., Jayne, J.T., Shi, Q., Kolb, C.E., Worsnop, D.R., Yourshaw, I., Seinfeld, J.H., Flagan, R.C., Zhang, X., Smith, K.A. and Morris, J.W.: Ambient aerosol sampling using the Aerodyne Aerosol Mass Spectrometer, J. Geophys. Res. - Atmos., 108 (D7), 1984-2012, doi:10.1029/2001jd001213, 2003.

John, W., Wall, S. M., Ondo, J. L., and Winklmayr, W.: Modes in the size distributions of atmospheric inorganic aerosol, Atmos. Environ., 24A, 2349-2359, 1990.

Meng, Z. and Seinfield, J. H.: On the source of the submicrometer droplet mode of urban and regional aerosols, Aerosol Sci. Tech., 20, 253-265, 1994.

Middlebrook, A. M., Bahreini, R., Jimenez, J. L. and Canagaratna, M. R.: Evaluation of Composition-Dependent Collection Efficiencies for the Aerodyne Aerosol Mass Spectrometer using Field Data, Aerosol Sci. Tech., 46, 258-271, doi:10.1080/02786826.2011.620041, 2012.

Moise,T., Flores, J.M., Rudich, Y.: Optical Properties of Secondary Organic Aerosols and Their Changes by Chemical Processes, Chem. Rev., 115.10, 4400-4439, doi: 10.1021/cr5005259, 2015.

Moosmüller, H., Chakrabarty, R. K., Ehlers, K. M., and Arnott, W. P.: Absorption Ångström coefficient, brown carbon, and aerosols: basic concepts, bulk matter, and spherical particles, Atmos. Chem. Phys., 11, 1217-1225, doi:10.5194/acp-11-1217-2011, 2011.

Ng, N. L., Canagaratna, M. R., Zhang, Q., Jimenez, J. L., Tian, J., Ulbrich, I. M., Kroll, J. H., Docherty, K. S., Chhabra, P. S., Bahreini, R., Murphy, S. M., Seinfeld, J. H., Hildebrandt, L., Donahue, N. M., DeCarlo, P. F., Lanz, V. A., Prévôt, A. S. H., Dinar, E., Rudich, Y., and Worsnop, D. R.: Organic aerosol components observed in Northern Hemispheric datasets from Aerosol Mass Spectrometry, Atmos. Chem. Phys., 10, 4625-4641, doi:10.5194/acp-10-4625-2010, 2010.

Ng, N. L., Canagaratna, M. R., Jimenez, J. L., Chhabra, P. S., Seinfeld, J. H., and Worsnop, D. R.: Changes in organic aerosol composition with aging inferred from aerosol mass spectra, Atmos. Chem. Phys., 11(13), 6465-6474, 2011.

Powelson, M.H., Espelien, B.M., Hawkins, L.N., Galloway, M.M., De Haan, D.O.: Brown carbon formation by aqueous-phase carbonyl compound reactions with amines and ammonium sulfate, Environ. Sci. Technol., 48 (2), 985-993, doi: 10.1021/es4038325, 2014.

Russell, P. B., Bergstrom, R. W., Shinozuka, Y., Clarke, A. D., DeCarlo, P. F., Jimenez, J. L., Livingston, J. M., Redemann, J., Dubovik, O., and Strawa, A.: Absorption Angstrom Exponent in AERONET and related data as an indicator of aerosol composition, Atmos. Chem. Phys., 10, 1155-1169, doi:10.5194/acp-10-1155-2010, 2010.

Saleh, R., Hennigan, C. J., McMeeking, G. R., Chuang, W. K., Robinson, E. S., Coe, H., Donahue, N. M., and Robinson, A. L.: Absorptivity of brown carbon in fresh and photo-chemically aged biomass-burning emissions, Atmos. Chem. Phys., 13, 7683-7693, doi:10.5194/acp-13-7683-2013, 2013.

Saleh, R., Robinson, E. S., Tkacik, D. S., Ahern, A. T., Liu, S., Aiken, A. C., Sullivan, R. C., Presto, A. A., Dubey, M. K., Yokelson, R. J., Donahue, N. M., and Robinson, A. L.: Brownness of organics in aerosols from biomass burning linked to their black carbon content, Nat. Geosci., 7, 647-650, 2014.

Seinfeld, J. H. and Pandis, S. P.: Atmospheric Chemistry and Physics, 2nd edn., John Wiley, New York, USA, 1232 pp., 2006.

5   Shapiro, E. L., Szprengiel, J., Sareen, N., Jen, C. N., Giordano, M. R., and McNeill, V. F.: Light-absorbing secondary organic material formed by glyoxal in aqueous aerosol mimics, Atmos. Chem. Phys., 9, 2289-2300, doi:10.5194/acp-9-2289-2009, 2009.

Shinozuka, Y., Clarke, A. D., DeCarlo, P. F., Jimenez, J. L., Dunlea, E. J., Roberts, G. C., Tomlinson, J. M., Collins, D. R., Howell, S. G., Kapustin, V. N., McNaughton, C. S., and Zhou, J.: Aerosol optical properties relevant to regional remote sensing of CCN activity and links to their organic mass fraction: airborne observations over Central Mexico and the US West Coast during MILAGRO/INTEX-B, Atmos.

10   Chem. Phys., 9, 6727-6742, doi:10.5194/acp-9-6727-2009, 2009.

Song, C., Gyawali, M., Zaveri, R.A., Shilling, J.E., Arnott, W.P.: Light absorption by secondary organic aerosol from α-pinene: Effects of oxidants, seed aerosol acidity, and relative humidity, J. Geophys. Res., 118 (20), 11741-11749, doi: 10.1002/jgrd.50767, 2013.

Virkkula, A., Ahlquist, N. C., Covert, D. S., Arnott, W. P., Sheridan, P. J., Quinn, P. K., and Coffman, D. J.: Modification, calibration and a field test of an instrument for measuring light absorption by particles, Aerosol Sci. Tech., 39, 68–83, 2005.

15   Virkkula, A.: Correction of the calibration of the 3-wavelength Particle Soot Absorption Photometer (3λPSAP), Aerosol Sci. Tech., 44, 706–712, 2010.

Zhang, X., Y.-H. Lin, J. D. Surratt, and R. J. Weber: Sources, composition and absorption angström exponent of light-absorbing organic components in aerosol extracts from the Los Angeles Basin, Environ. Sci. Technol., 47(8), 3685-3693, 2013.
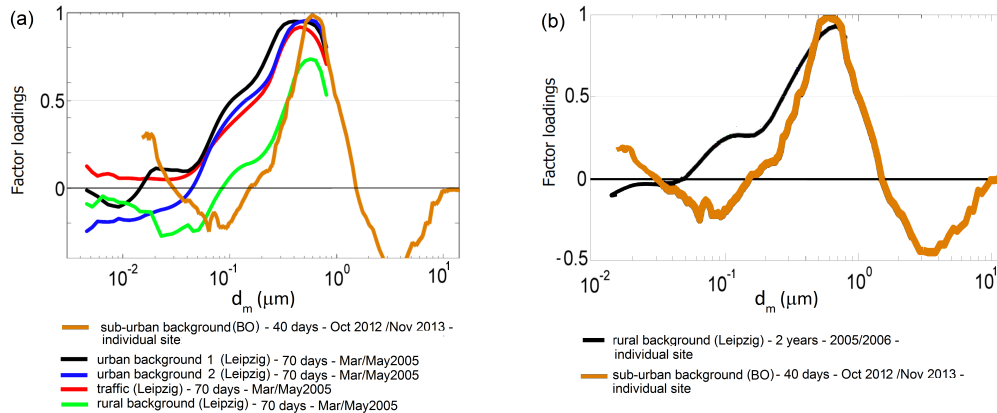
Figure 1. The "droplet" mode of the particle number size distribution (PNSD). Factor loadings calculated by PNSD Principal Component Aanalysis (PCA) are plotted against electrical mobility particle diameter (d_m). Factor loadings are PCA statistical variables indicating correlations between PNSDs and the droplet mode PCA component. Data from this study (brown line) are compared with data obtained by Costabile et al. (2009) in Leipzig (Germany) at: (a) combined urban sites for 70 days in Spring 2005 (green, blue, red, and black lines, as indicated in the legend), and (b) a single site from long-term (2 years) measurements (black line).
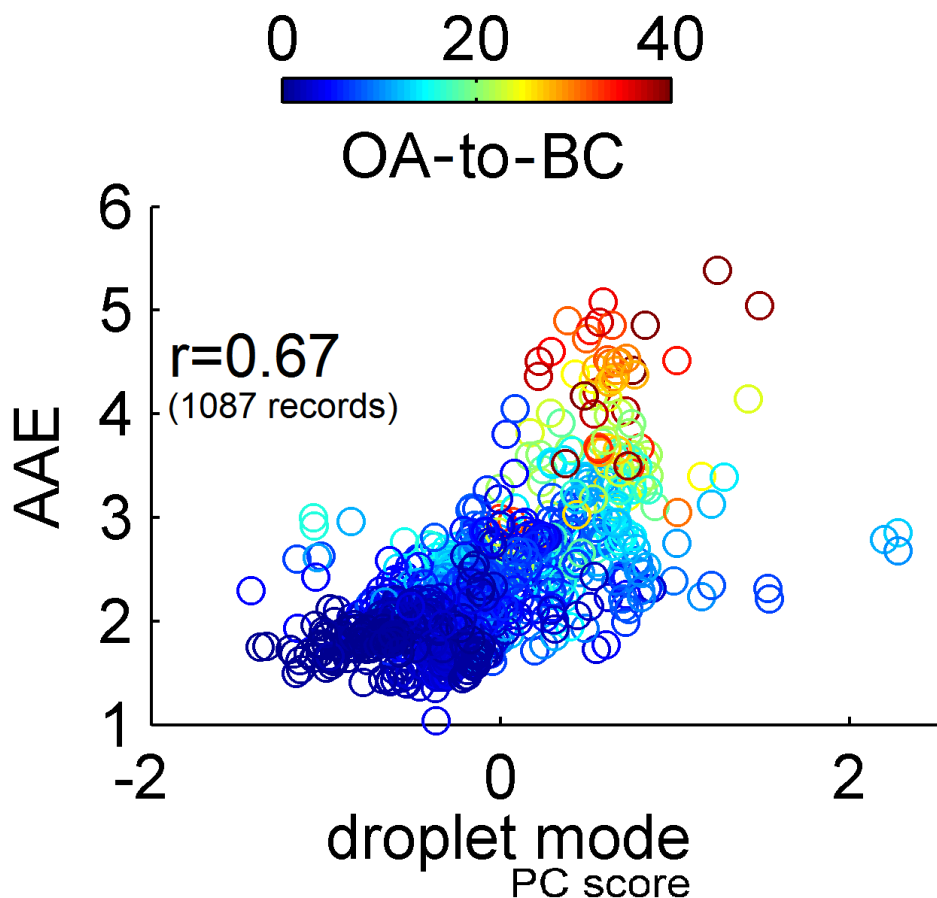
Figure 2. Correlation plot between Absorption Angstrom Exponent at 467-660 nm (AAE), and the "droplet mode" aerosol (x-axis is the score of the principal component (PC) representing the droplet mode aerosol). Data color is the Organic Aerosol to Black Carbon ratio (OA-to-BC). The Pearson's correlation coefficient (r) is indicated.
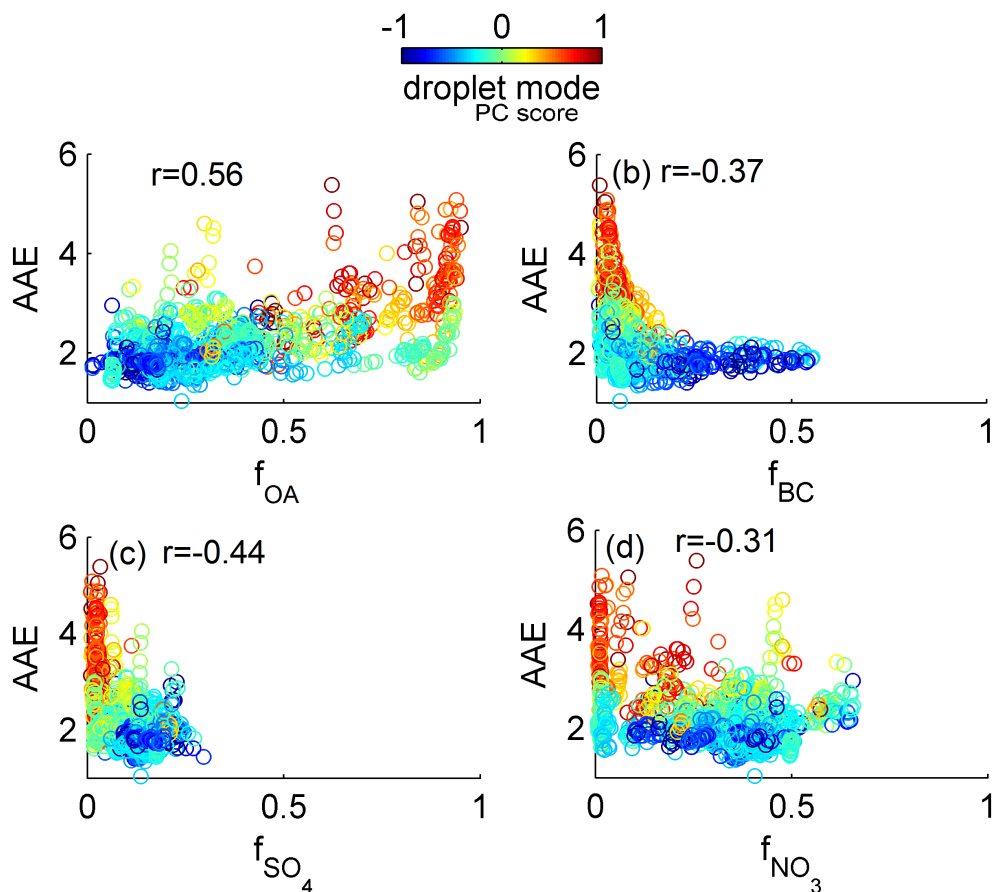
Figure 3. Correlation plots between Absorption Angstrom Exponent at 467-660 nm (AAE), and mass fractions of (a) organic aerosol (f_{OA}), (b) Black Carbon (f_{BC}), (c) sulfate (f_{SO_4}), and (d) nitrate (f_{NO_3}). Data color is the score of the droplet mode aerosol. Relevant Pearson's correlation coefficients (r) are indicated.
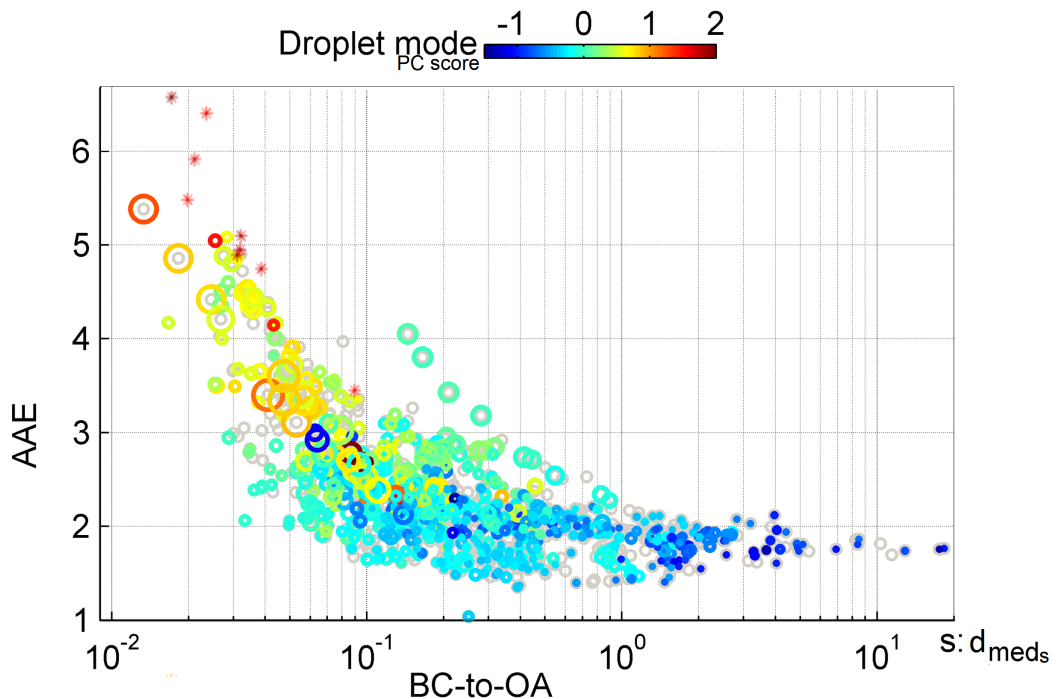
Figure 4. Relation between "brown aerosol" and Black Carbon (BC) to Organic Aerosol (OA) ratio (BC-to-OA). Absorption Angstrom Exponent at 467-660 nm (AAE) is plotted against BC-to-OA. Data color is the score of the droplet mode PC extracted by the statistical analysis. Data size is the median diameter of the particle surface size distribution ($d_{med(S)}$). Data indicated by "*" show case-study values illustrated in Fig. 5. Grey dots represent all data measured, while colored dots are the subset of these data including statistically significant values of droplet mode PC scores.
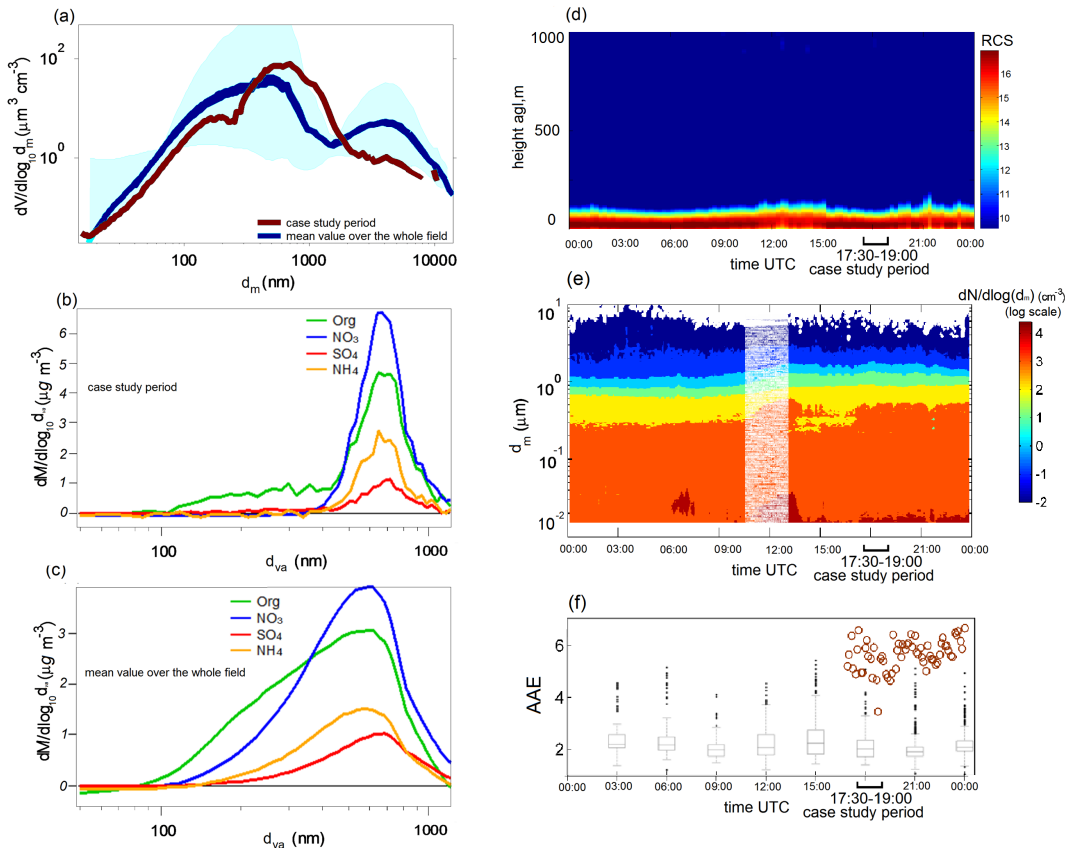
Figure 5. A case-study illustrating major features of the "brown aerosol". Case-study period is the first of February,2013, from 17:30 to 19:00 UTC. Case-study values are compared with mean values over the whole field experiment. Panels illustrate: (a) particle volume size distribution (dV/dlog$_{10}$d$_m$, based on electrical mobility particle diameter d$_m$) during the case-study and relevant mean values; (b) particle mass size distribution (dM/dlog$_{10}$d$_{va}$, based on vacuum aerodynamic diameter, d$_{va}$) during the case-study, and (c) relevant mean values; (d) aerosol vertical profiles in the atmosphere during the case-study day (time-height cross section of the range corrected signal, RCS=ln(S×R^2), from a LD40 ceilometer); (e) particle number size distributions during the case-study day (whiter area includes corrupted data); (f) Absorption Angstrom Exponent at 467-660 nm (AAE) during the case study day (brown circles), and relevant statistical values during the whole field (grey box plots, showing median, percentiles, and outliers).
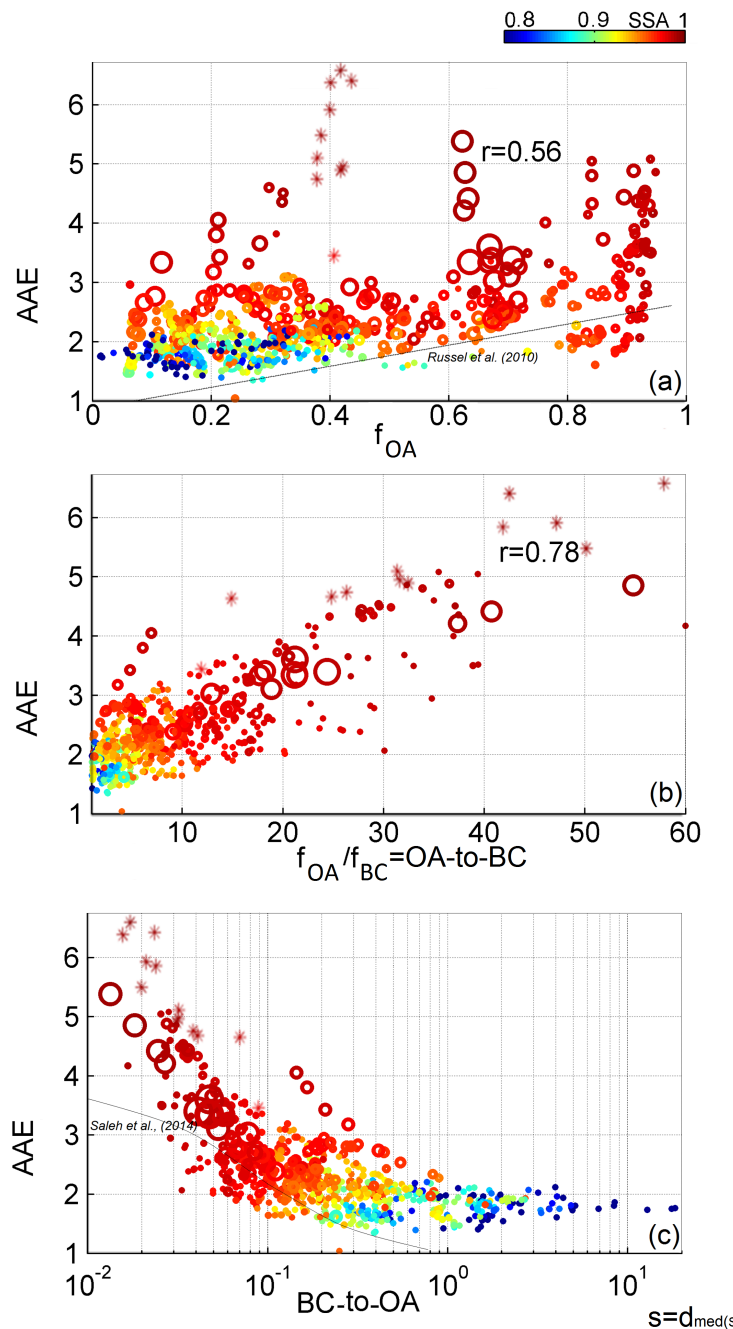
Figure 6. Dependence of Absorption Angstrom Exponent at 467-660 nm (AAE) on (a) organic aerosol mass fraction (f_{OA}), (b) Organic Aerosol (OA) to Black Carbon (BC) ratio (OA-to-BC), and (c) BC-to-OA ratio. Data color is Single Scattering Albedo at 530 nm. Data size is median diameter of particle surface size distributions (d_{med_S}, ranging from 50 to 300 nm). Data indicated by "*" show case study values illustrated in Fig. 5. Relevant Pearson's correlation coefficients (r) are indicated. Previous results by Russell et al. (2010) and Saleh et al. (2014) are indicated by light lines in panels a and c, respectively.
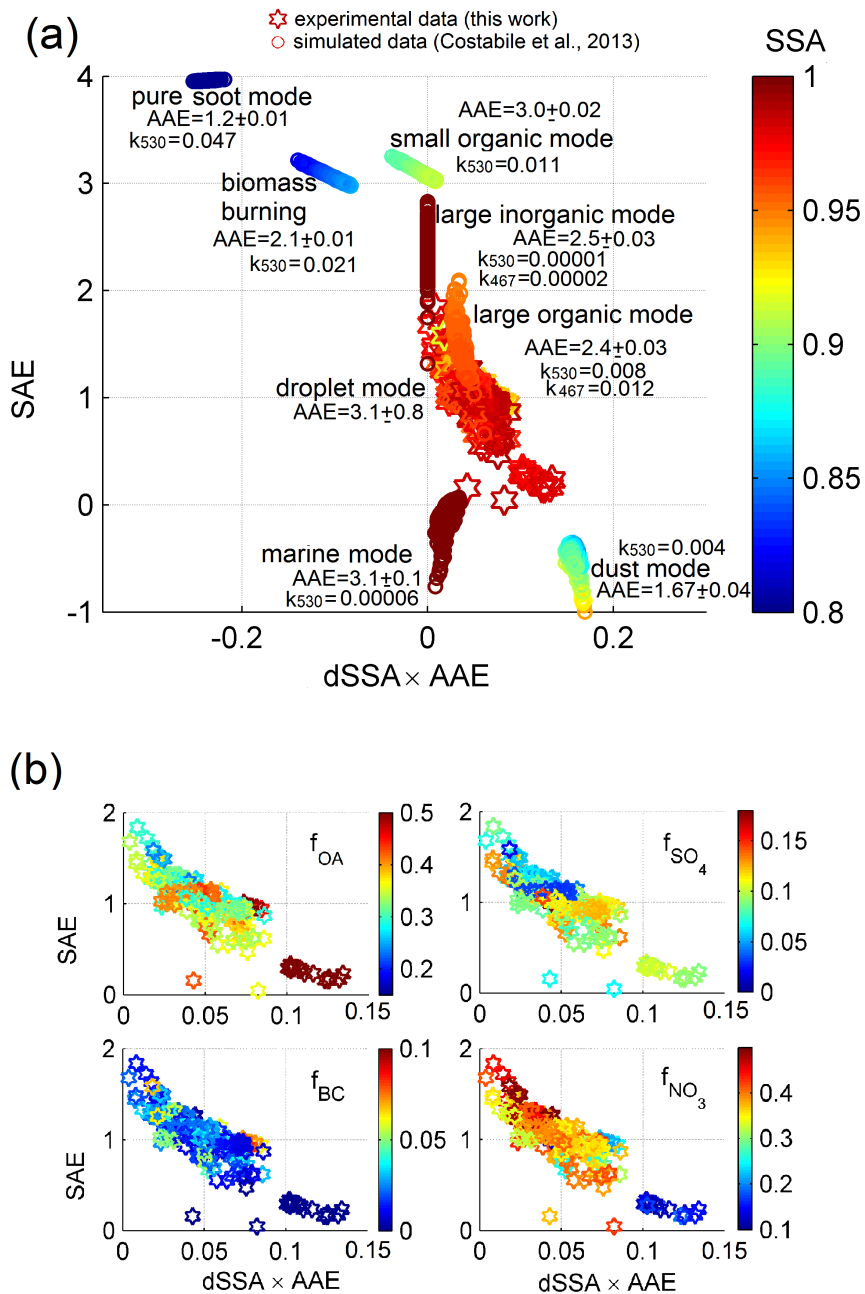
Figure 7. Optical signature of the "brown aerosol" as indicated by the paradigm proposed by Costabile et al. (2013). Absorption Angstrom Exponent at 467-660 nm (AAE) times spectral variation of Single Scattering Albedo from 660 to 467 nm (dSSA = SSA_{660} - SSA_{467}) is plotted against Scattering Angstrom Exponent at 467-660 nm (SAE). Panel (a) shows experimental data of the droplet mode obtained in this work (representing the brown aerosol) in comparison with key aerosol types obtained through Mie simulations. Data color is SSA at 520 nm. Relevant AAE values for key aerosol types are indicated as mean±standard deviation. Panel (b) zooms in panel a to show the "brown" aerosol optical properties variability with varying major PM_1 mass fractions (f_{OA}, f_{BC}, f_{SO_4}, f_{NO_3}).
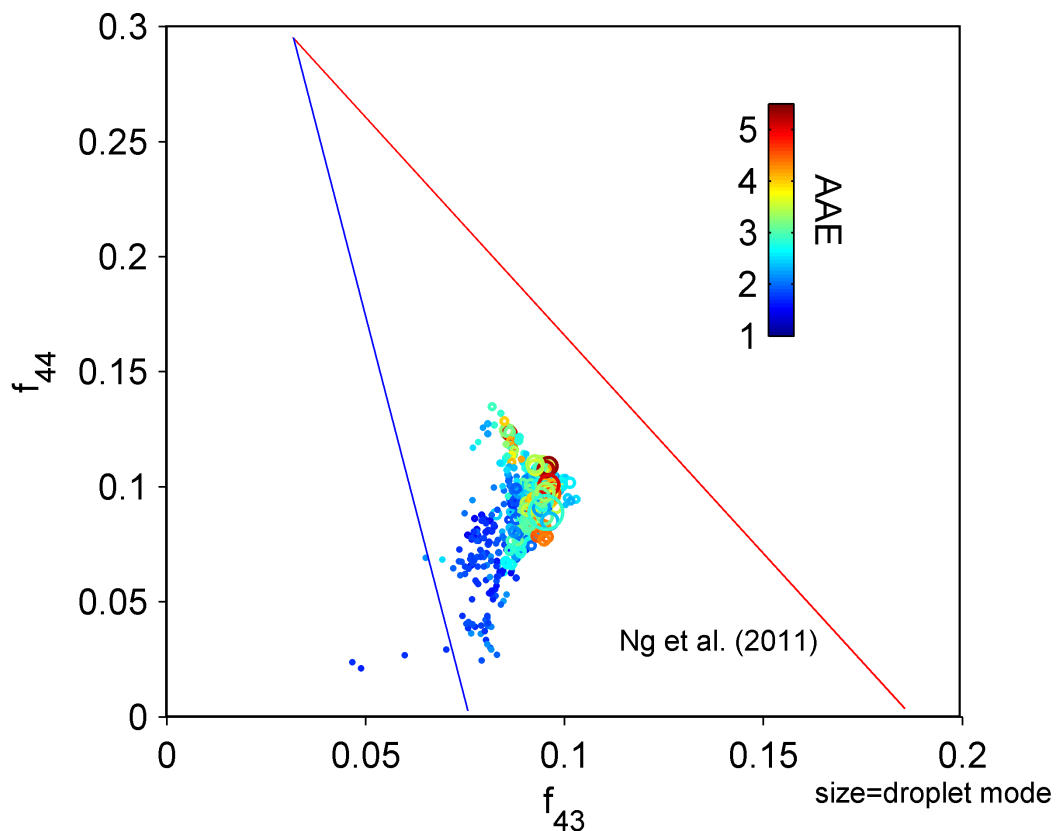
Figure 8. "Triangle plot" reproduced from Ng et al. (2011) for the "brown" aerosol. f_{44} is plotted against f_{43}, data color being the Absorption Angstrom Exponent at 467-660 nm (AAE), and data size the droplet mode score. The triangular space indicated by red and blue lines shows where the majority of OA values measured in ambient samples fall into.

Table 1. Pearson's correlation coefficients (r) between: Absorption Angstrom Exponent (AAE); scores of principal components (PC1-PC4) of particle number size distributions obtained by Principal Component Analysis (PCA); mass fractions of Black Carbon (f_{BC}), organics (f_{OA}), nitrate (f_{NO3}), sulfate (f_{SO4}), and ammonium (f_{NH4}); median diameter of the particle surface size distribution ($d_{med(S)}$); BC mass concentration (BC); organic aerosol (OA) to BC ratio (OA-to-BC); ratio of the AMS signal at m/z 44 and m/z 43 to the total organics AMS signal (f_{44} and f_{43}). Note that PC3 is the "droplet" mode PC.

r	AAE	$d_{med(S)}$	BC	f_{BC}	f_{OA}	OAtoBC	f_{NO3}	f_{SO4}	f_{NH4}	f_{44}	f_{43}
AAE		0.48	-0.26	-0.37	0.56	0.78	-0.31	-0.44	-0.41	0.45	0.45
PC1	0.14	-0.02	0.60	0.31	0.08	0.00	-0.1	-0.35	-0.22	-0.20	-0.25
PC2	-0.18	-0.18	-0.01	0.20	0.09	-0.08	-0.15	-0.15	-0.18	-0.07	0.15
PC3	0.67	0.60	-0.35	-0.42	0.64	0.60	-0.35	-0.49	-0.47	0.42	0.67
PC4	-0.13	-0.34	-0.04	0.19	-0.20	-0.14	0.15	0.03	0.16	0.03	0.24
$d_{med(S)}$	0.48		0.22	-0.48	0.38	0.48	-0.12	-0.25	-0.18		